Website 1

The American Heritage® Dictionary of the English Language: Fourth Edition. 2000.

epitaxy

SYLLABICATION: ep·i·tax·y

PRONUNCIATION: ĕp'ĭ-tăk'sē

NOUN: Inflected forms: pl. **ep·i·tax·ies**
The growth of the crystals of one mineral on the crystal face of another mineral, such that the crystalline substrates of both minerals have the same structural orientation.

CONTENTS · INDEX · ILLUSTRATIONS · BIBLIOGRAPHIC RECORD
< epitasis epithalamium >

Website 2

大石 耕一郎 助教授の現在の研究課題

カルコパイライト化合物のエピタキシャル成長に関する研究

カルコパイライト化合物は、主に光電子素子用材料として研究されている物質です。現在、薄膜太陽電池材料としての研究・開発が最も進んでいます。

エピタキシャル成長とは、単結晶基板上に薄膜結晶が成長する際に、薄膜が基板結晶の方位に影響されて、ある特定の方位に成長する現象のことです。通常、物質の電気的・光学的特性は薄膜化すると低下してしまいますが、もし完全な単結晶膜を成長することができれば、物質本来の特性を維持することができ、素子としての応用が広がります。

この研究では、半導体の代表格であるシリコン(Si)やガリウム砒素(GaAs), ガリウムリン(GaP)基板上にカルコパイライト化合物を薄膜成長し、それらの組み合わせることで、今までにない高機能・新機能の素子の実現を目指しています。

図1に示すように、カルコパイライト構造は立方晶系のダイヤモンド構造や閃亜鉛鉱構造に類似していますが、これらを二段重ねしたような正方晶系の結晶構造です。立方晶系の(100)基板上に正方晶系の膜を成長させる場合、膜の成長が基板の方位の影響を受けるのであれば、幾何学的には図2のような配向が考えられます。

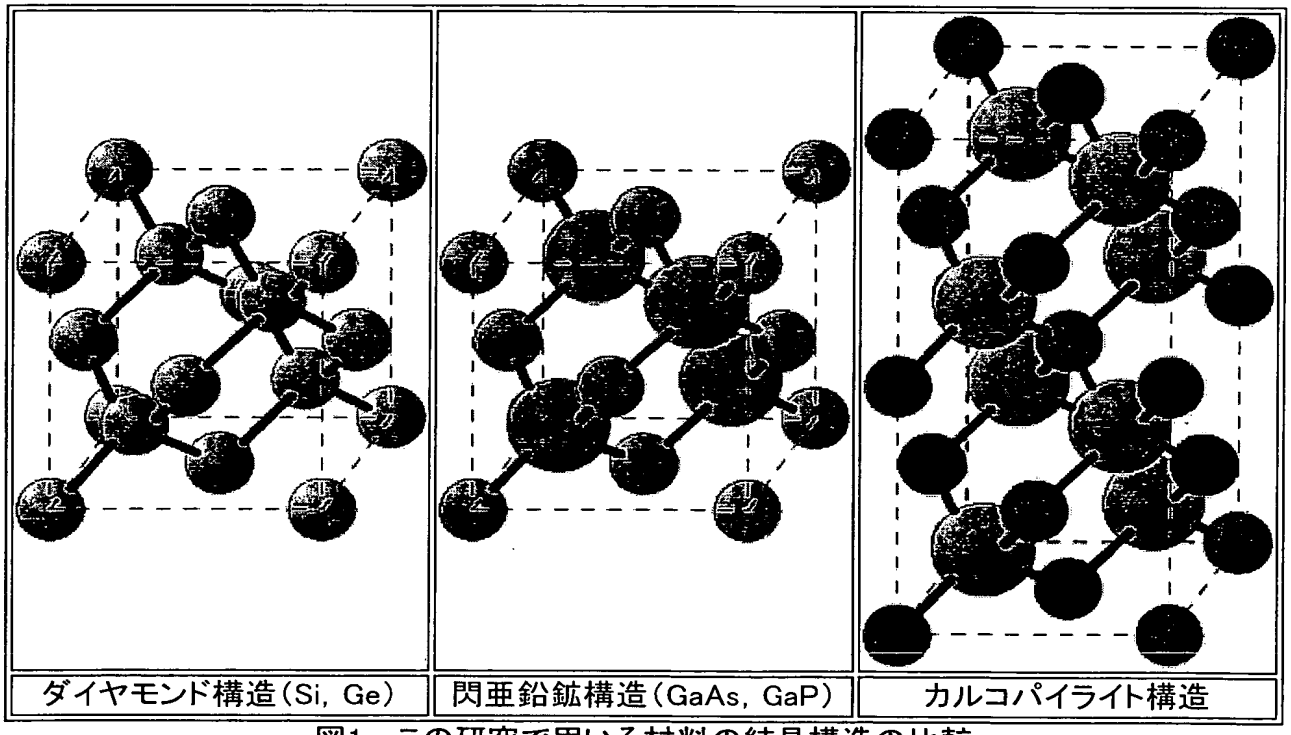

図1. この研究で用いる材料の結晶構造の比較

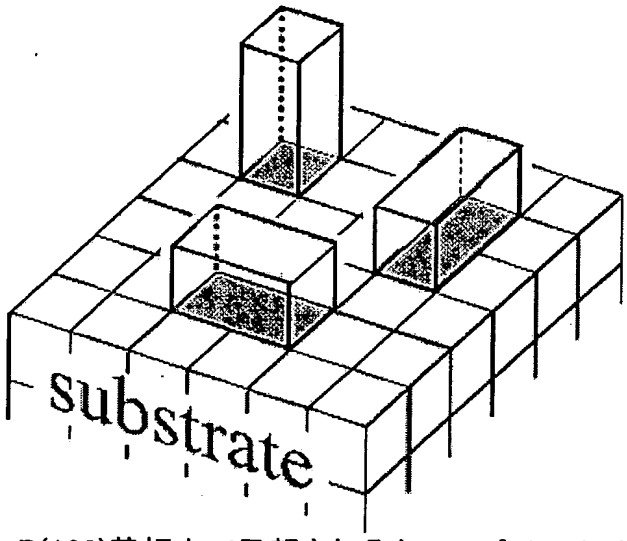

図2. Si, GaAs, GaP(100)基板上で予想されるカルコパイライト化合物薄膜の配向

これまでは、カルコパイライト化合物の$CuGaS_2$を、主にSi(100)基板上に成長させる研究をしてきました。X線回折や反射高速電子線回折(Reflection High Energy Election Diffraction: RHEED)を用いた結晶学的評価を中心に行い、図3や図4のような膜の配向の様子を明らかにしました。

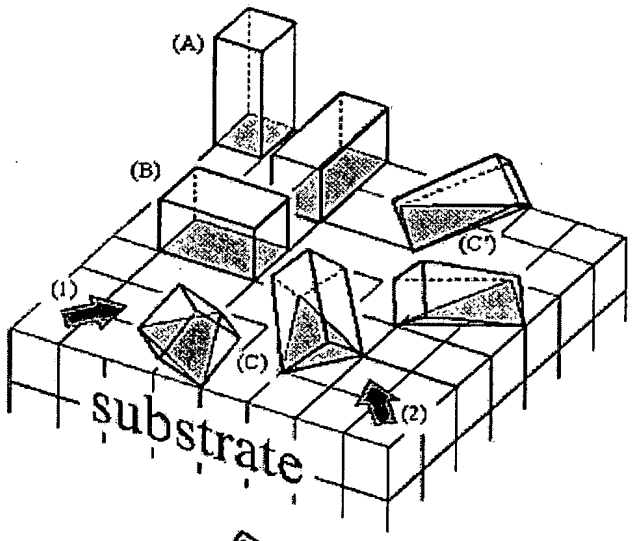

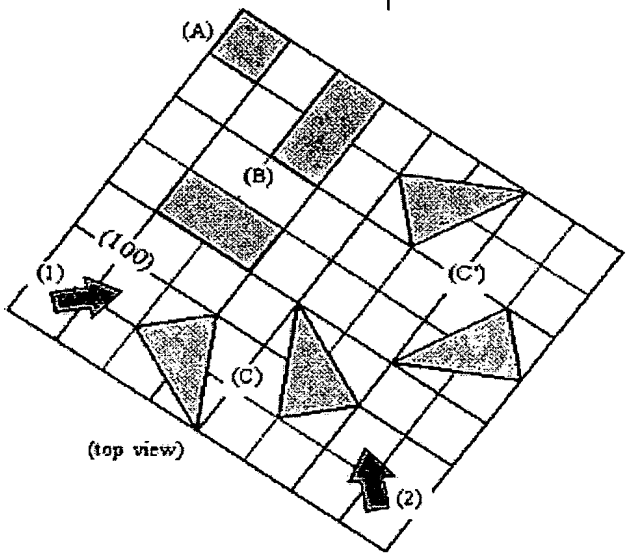

図3. Si(100)基板上に成長した$CuGaS_2$薄膜の配向の様子(解析結果)

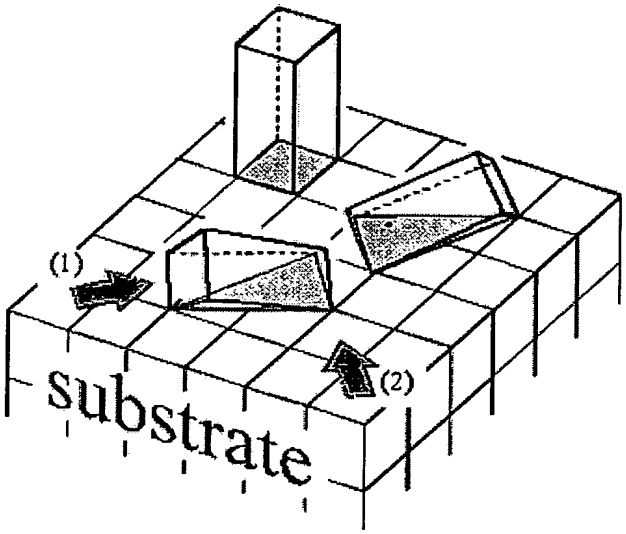

図4. GaAs, GaP(100)基板上に成長した$CuGaS_2$薄膜の配向の様子(解析結果)

現在は、カルコパイライト化合物の$CuInS_2$と太陽電池材料としても最も一般的なSiを組み合わせて、エネルギー変換効率を上げることができないか検討しています。$CuInS_2$は、その光学的性質が太陽電池材料として魅力的な物質ですが、Siと組み合わせるという発想は、

- 現在最も普及しており、またすでに技術が確立しているシリコン太陽電池とタンデム化することで、エネルギー変換効率を向上させることができる可能性がある。
- 構成元素である銅(Cu), インジウム(In), 硫黄(S)のいずれも、毒性の強い物質ではない。

という点に着目しています。

反射高速電子線回折による薄膜結晶の構造・配向評価

- 薄膜の結晶学的評価はX線回折だけで充分でしょうか？

電子材料の研究・開発において、結晶学的な評価は不可欠です。一口に"結晶学的評価"といっても、様々な手法がありますが、バルク試料に対する最も一般的な評価方法は、X線回折による$2\theta-\theta$スキャン測定の解析といってよいでしょう。

しかし、2θ－θX線回折では、単結晶やエピタキシャル膜などの結晶方位を議論するための充分な情報は得ることができません。2θ－θX線回折は、粉末X線回折法とも呼ばれるように、本来、粉末結晶試料の同定を目的としており、測定データのピーク位置及び強度比を標準となるASTMカードと比較することで評価しますが、単結晶やエピタキシャル(またはいくつかの限られた配向をだけを持った)膜の測定データは、回折ピークの数が少ないので、ピーク位置の情報しか利用することができないからです。

さて、上の問いかけに対する答えですが、薄膜結晶の構造・配向評価用に設計されたX線回折装置が

手元にあるのであれば、 YES
そういったものを持っていなければ、NO

となります。

- 反射高速電子線回折(Reflection High Energy Election Diffraction: RHEED)とは...

反射高速電子線回折(Reflection High Energy Election Diffraction: RHEED)を説明するためには、"逆格子(reciprocal lattice)"と"エワルド球(Ewald sphere)"の概念を導入しなければなりません。

面間隔dの結晶面に、入射角θと同じ角度で散乱されたX線または電子線の波は、ブラッグ(Bragg)の回折条件

$$2d\sin\theta = n\lambda$$

が満たされたときに位相が揃って強め合います。

一方、RHEEDやX線回折の"逆格子マッピング"では、逆格子とエワルド球の概念を用いて、回折現象を2次元的に観察することになります。図5は、逆格子とエワルド球の関係を示したものです。逆格子は、物質の結晶構造がわかれば、作図することができます。kやk'は、入射波と反射波の波数ベクトルです(大きさは、使用するX線の波長や電子線の加速電圧によって決まってきます)。

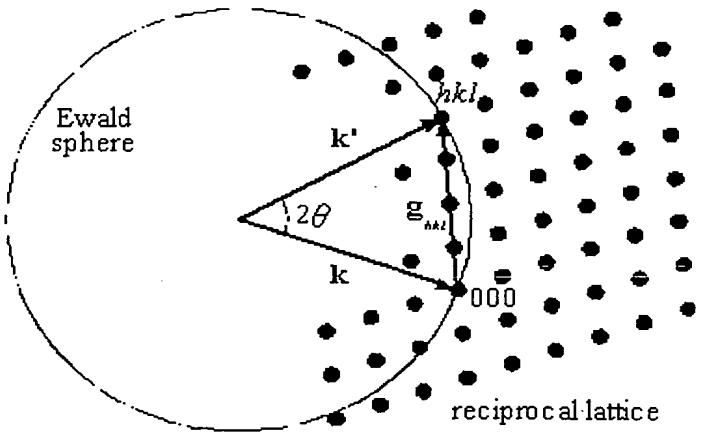

図5. 逆格子とエワルド球

図5において、エワルド球上の逆格子点hklに対応する格子面は、ブラッグの回折条件を満たしています。ここまでは、X線回折も電子線回折も同じです。

RHEEDとX線回折の違いは、エワルド球の大きさにあります。RHEEDのエワルド球は、逆

格子からは平面とみなせるほど非常に大きいので、原点付近の逆格子が、そのままスクリーンに投影されます。

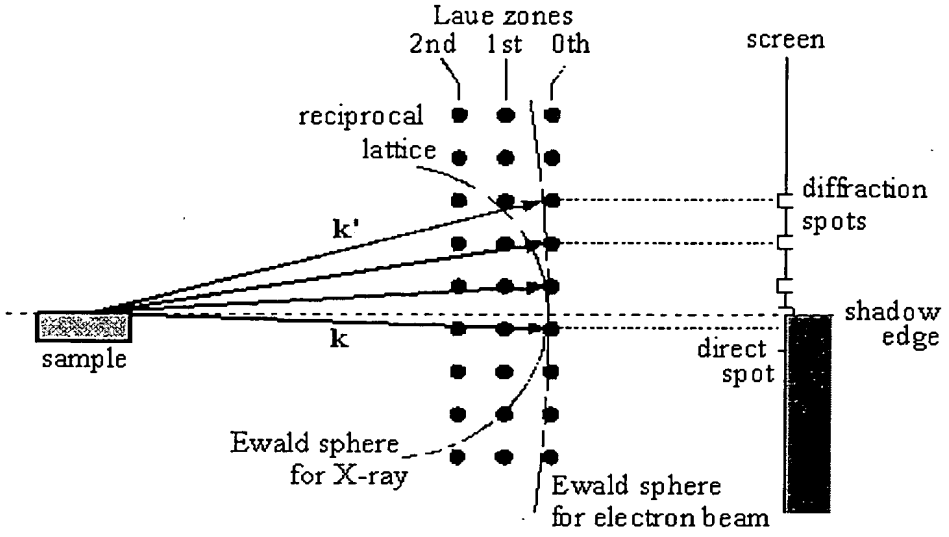

図6. RHEEDにおける逆格子とエワルド球の関係

結晶の逆格子は、結晶構造と単位胞内の個々の原子の座標がわかれば計算することができるので、逆格子シミュレーションと観察したRHEEDパターンを用いて、結晶構造や配向に関する詳細な解析を行うことができます。

- 解析例(試料:Si(100)基板上に成長した$CuGaS_2$薄膜)

2θ−θX線回折だけで配向評価を行うと、図7のようになります。上のX線回折パターンは、(A)と(B)の配向の混在を、下のパターンは(A)の配向のみを示しています。

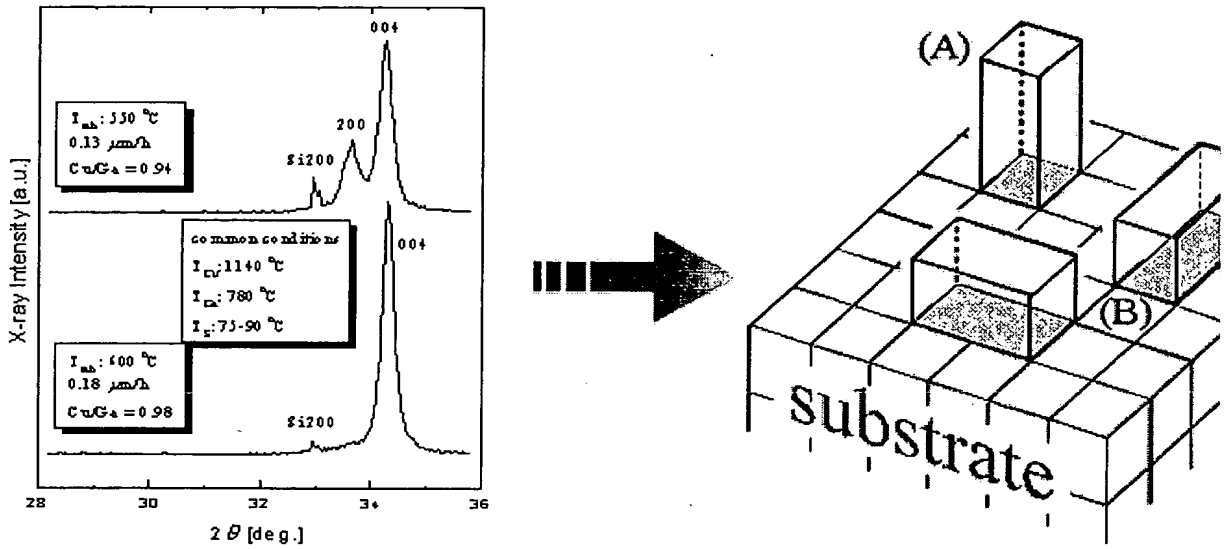

X線回折パターン　　解析結果

図7. 2θ−θX線回折による配向評価

一方、カルコパイライト化合物の結晶構造や個々の原子の座標はわかっているので、配

向を図2のように幾何学的に想定すると、試料のRHEEDパターンを図8のようにシミュレーションすることができます。

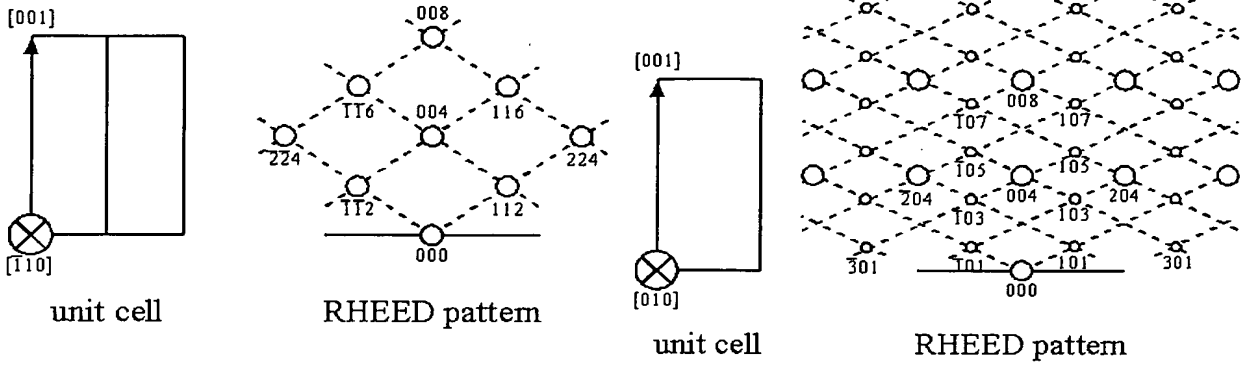

(A)の配向に対するパターンシミュレーション

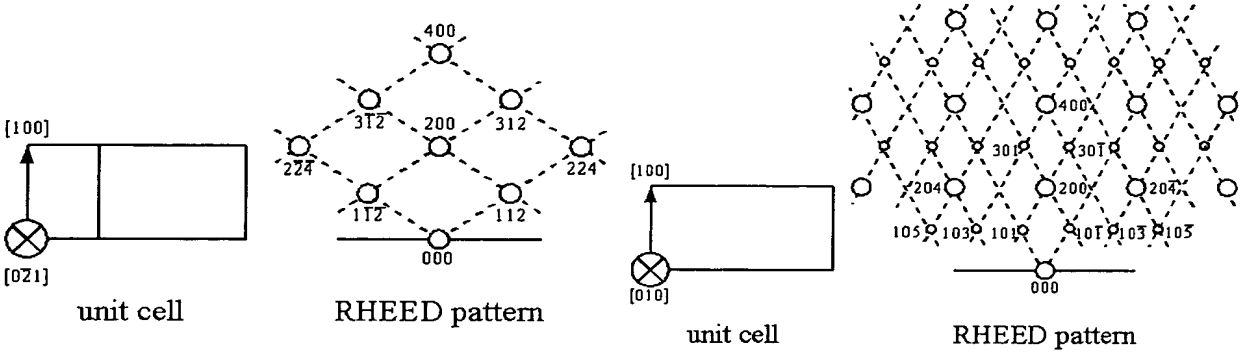

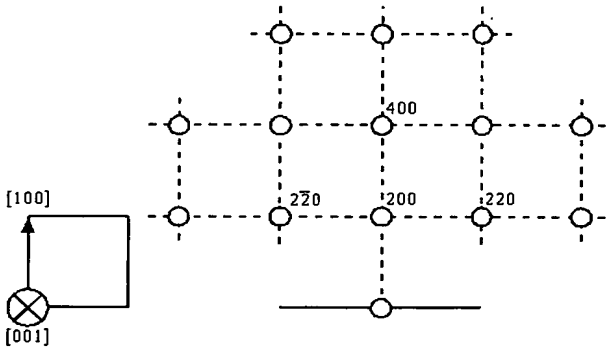

(B)の配向に対するパターンシミュレーション

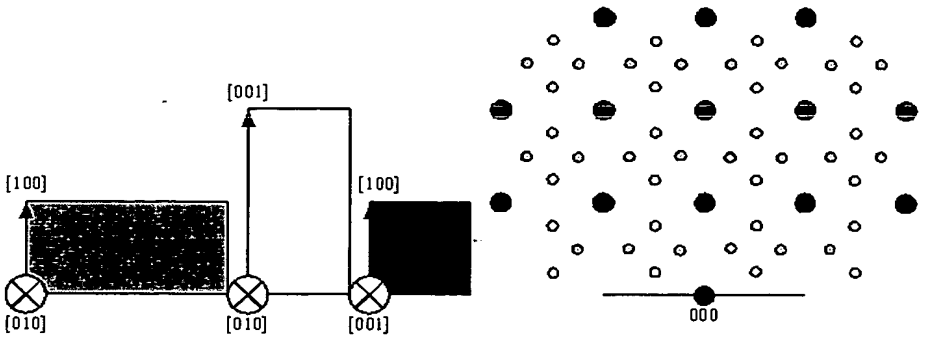

(A)と(B)の配向が混在する場合

図8. RHEEDパターンのシミュレーション

図9のようなX線回折パターンを示す試料の場合、図7の(A)の配向が考えられますが、実際のRHEEDパターンは、図8のシミュレーションとは一致しませんでした。

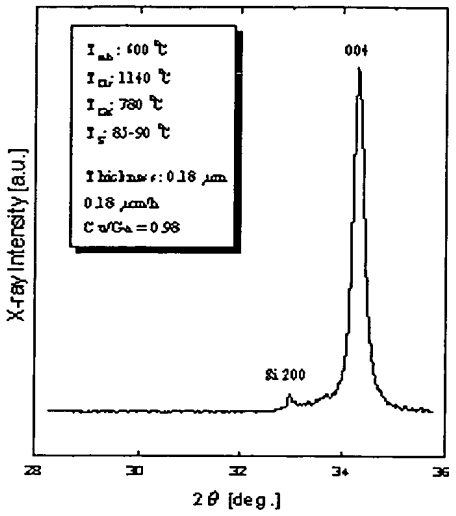

X線回折パターン

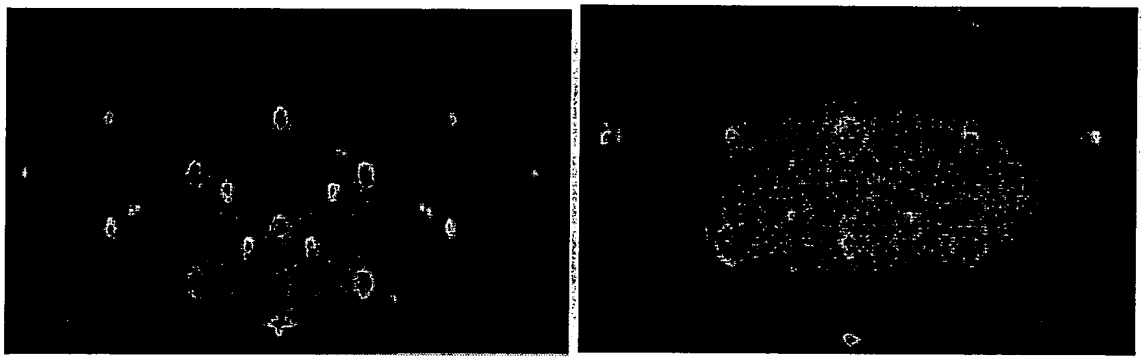

RHEEDパターン

図9. 同一試料のX線回折パターンとRHEEDパターン

このRHEEDパターンについて、図8のシミュレーションに図10のような解析を加えた結果、配向状態は図3のようになっているという結論に達しました。

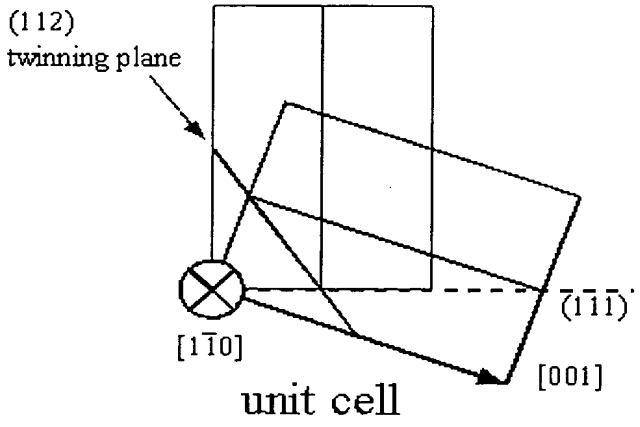

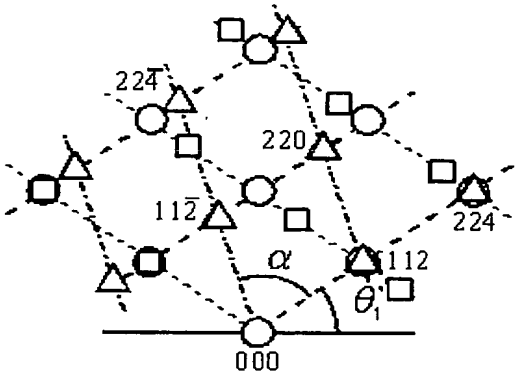

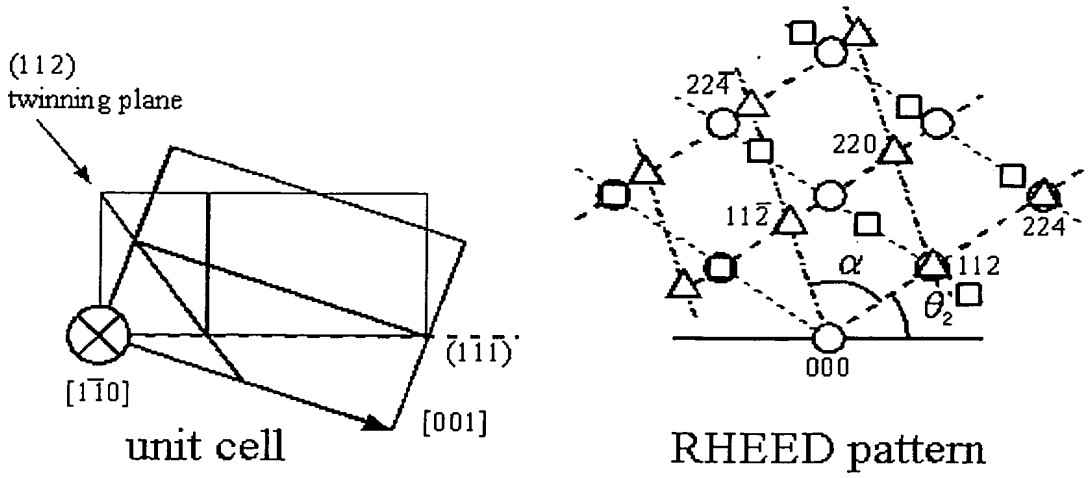

図10. RHEEDパターンの解析

以上の解析は、試料の結晶構造，格子定数と単位胞内の個々の原子の座標がわかれば、ベクトルの作図とExcelなどを用いた計算で行うことができます。

Translation of www.nagaoka-ct.ac.jp/me/oishi/research.html

Subject of Current Study by Assistant Professor, Mr. Koichro Oishi

Study on epitaxial growth of chalcopyrite compound

Chalcopyrite compounds are materials on which study has been promoted as materials to be used mainly in photoelectronic elements. Research and development thereof as a material of thin film solar cells have been advanced the most.

Epitaxial growth is a phenomenon that in growing crystals of a thin film on a monocrystal substrate, the crystals is grown in a specified orientation under the influence of the crystal orientation of the substrate. Normally, electrical and optical characteristics of a material lower when undergoing thin film fabrication. However, if a complete monocrystal film could be grown, the inherent characteristics of the material are maintained, attaining wide application to various kinds of elements.

The present study aims at realizing an element having an unprecedented, enhanced function by combining thin films of chalcopyrite compounds grown on a substrate of typical semiconductors, silicon (Si), gallium arsenide (GaAs), and gallium phosphide (GaP).

As shown in FIG. 1, though it is analogous to diamond structure and zinc blend structure of cubic systems, the chalcopyrite structure is a crystal structure of a tetragonal system like one in which these two structures are stucked. In growing a film of a tetragonal system on a (100) substrate of a cubic system, it is expected that the orientation as shown in FIG. 2 is obtained geometrically when the orientation of the substrate affects the film growth.

FIG. 1 Comparison of crystal structures among materials used in the present study
Diamond structure (Si/Ge) Zinc blend structure (GaAs/GaP) Chalcopyrite structure

FIG. 2 Orientation in chalcopyrite compound thin film expected to be grown on Si/GaAs/GaP (100) substrate

To date, I have dominantly devoted myself to study for growing $CuGaS_2$ as a chalcopyrite compound on a Si (100) substrate. My study has concentrated on crystallographic evaluation using X-ray diffraction and reflection high energy electron diffraction (RHEED) to reveal the orientations of the films as shown in FIG. 3 and FIG. 4.

FIG. 3 Orientation in $CuGaS_2$ thin film grown on Si (100) substrate (analysis result)

FIG. 4 Orientation in $CuGaS_2$ thin film grown on GaAs/GaP (100) substrate (analysis result)

At present, I am examining whether the energy conversion efficiency can be increased by combining $CuInS_2$ as a chalcopyrite compound with Si that is used generally the most as a material of solar cells. $CuInS_2$ is an attractive material in its optical characteristic as a material of solar cells, and the idea of combining $CuInS_2$ with Si is formed in view of the following points. Namely, my attention is directed to the following points:

- There is possibility of increasing the energy conversion efficiency by allowing the compound to be in tandem with a silicon solar cell which has been widespread the most and of which technology has been already established.
- None of the structural elements, i.e., copper (Cu), indium (In), and sulfur (S) exhibit strong toxicity.

Structure/orientation evaluation of thin film crystals by reflection high energy electron diffraction

- Is crystallographic evaluation of thin films only by X-ray diffraction sufficient?

Crystallographic evaluation is essential in research and development of electronic materials. For the "crystallographic evaluation," there are various kinds of methods, and the most general evaluation method for bulk samples may be an analysis of 2θ-θ scan measurement by the X-ray diffraction.

In the 2θ-θ X-ray diffraction, however, insufficient information for discussing and examining the crystal orientations of the monocrystal and epitaxial films, and the like is obtained. The reason is that: while the 2θ-θ X-ray diffraction, which is some times called powder X-ray diffraction, originally aims at identification of powder crystal samples and performs evaluation by comparing peak points and intensity ratios between measurement data and an ASTM card as a reference, the measurement data of the monocrystal and epitaxial films (and films having some specified orientations) includes less number of diffraction peaks and only information on peak points can be utilized accordingly.

Referring to the above-mentioned question, if an X-ray diffraction system designed for structure/orientation evaluation of thin film crystals is:

available, the answer is YES; or
not available, the answer is NO.

- What is reflection high energy electron diffraction (RHEED)?

For explaining the reflection high energy electron diffraction (RHEED), the concepts of "reciprocal lattice" and "Ewald sphere" should be introduced.

When the condition of Bragg diffraction:

$$2d\sin\theta=n\lambda$$

is satisfied, waves of X-rays or electron beams scattered at the same angle as an incident angle θ on crystal planes at interplanar spacing d agree in their phase with the incident waves to be amplified.

Meanwhile, in "reciprocal lattice mapping" in the RHEED and the X-ray diffraction, diffraction phenomena are observed two-dimensionally by employing the concepts of the reciprocal lattice and the Ewald sphere. FIG. 5 shows the relationship between the reciprocal lattice and the Ewald sphere. The reciprocal lattice can be drafted with a crystal structure of a material. k and k' denote wave vectors of an incident wave and a reflected wave, respectively (each scale depends on the wavelength and the acceleration voltage of the X-ray or the electron beam to be used, and the like.).

FIG. 5 Reciprocal lattice and Ewald sphere

In FIG. 5, the lattice plane corresponding to the reciprocal lattice point *hkl* on the Ewald sphere satisfies the condition of Bragg diffraction. No difference lies between in the X-ray diffraction and in the electron diffraction up to this stage.

The scale of Ewald sphere is the difference between the RHEED and the X-ray diffraction. The Ewald sphere in the RHEED is so large that it can be regarded as a plane in the reciprocal lattice, and therefore, the reciprocal lattice around the origin is projected directly to a screen.

FIG. 6 Relationship between reciprocal lattice and Ewald sphere in RHEED

The reciprocal lattice of crystals can be calculated with the crystal structure and the coordinates of respective atoms within a unit cell, enabling detail analysis of the crystal structure and the orientation by performing reciprocal lattice simulation and using the observed RHEED pattern.

- Analysis example (sample: $CuGaS_2$ thin film grown on Si (100) substrate)

Orientation evaluation only by 2θ-θ X-ray diffraction results in FIG. 7. The upper X-ray diffraction pattern indicates orientation mixture of (A) and (B) while the

lower pattern indicates only orientation of (A).

FIG. 7 Orientation evaluation by 2θ-θ X-ray diffraction
X-ray diffraction pattern Analysis result

Meanwhile, the crystal structure and the coordinates of the respective atoms of the chalcopyrite compound are known. So, geometrical assumption of the orientation as shown in FIG. 2 enables simulation of the sample RHEED pattern as shown in FIG. 8.

FIG. 8 RHEED pattern simulation
Pattern simulation on orientation (A)
Pattern simulation on orientation (B)
Pattern simulation on orientation mixture of (A) and (B)

Though it had been expected that the sample indicating the X-ray diffraction pattern as shown in FIG. 9 has crystals in the orientation (A) in FIG. 7, the actually obtained RHEED pattern did not match with the pattern obtained by the simulation shown in FIG. 8.

FIG. 9 X-ray diffraction pattern and RHEED pattern obtained from the same sample
X-ray diffraction pattern
RHEED pattern

The result of the simulation as in FIG. 8 and the analysis as shown in FIG. 10 to this RHEED leads to a conclusion that the resultant orientation is as shown in FIG. 3.

FIG. 10 Analysis of RHED pattern

The above analysis can be performed by vector drafting and calculation using Excel or the like if the crystal structure, lattice constant, and coordinates of the respective atoms within the unit cell of the sample are known.

website3

APPLIED PHYSICS LETTERS VOLUME 79, NUMBER 7 13 AUGUST 2001

All-epitaxial fabrication of thick, orientation-patterned GaAs films for nonlinear optical frequency conversion

L. A. Eyres,[a] P. J. Tourreau,[b] T. J. Pinguet, C. B. Ebert,[c] J. S. Harris, and M. M. Fejer
Center for Nonlinear Optical Materials, Stanford University, Stanford, California 94305-4090

L. Becouarn,[d] B. Gerard, and E. Lallier
Laboratoire Central de Recherches, THALES, Domaine de Corbeville-91404 Orsay Cedex, France

(Received 19 February 2001; accepted for publication 12 June 2001)

Orientation-patterned GaAs (OPGaAs) films of 200 μm thickness have been grown by hydride vapor phase epitaxy (HVPE) on an orientation-patterned template fabricated by molecular beam epitaxy (MBE). Fabrication of the templates utilized only MBE and chemical etching, taking advantage of GaAs/Ge/GaAs heteroepitaxy to control the crystal orientation of the top GaAs film relative to the substrate. Antiphase domain boundaries were observed to propagate vertically under HVPE growth conditions so that the domain duty cycle was preserved through the thick GaAs for all domain periods attempted. Quasiphase-matched frequency doubling of a CO_2 laser was demonstrated with the beam confocally focused through a 4.6 mm long OPGaAs film. © *2001 American Institute of Physics.* [DOI: 10.1063/1.1389326]

Though GaAs has many advantageous characteristics for nonlinear optical frequency conversion including a large nonlinear susceptibility ($d_{14} \geqslant 90$ pm/V), transparency from 1.0 μm to beyond 12 μm, and a high thermal conductivity (46 W/m K), its isotropic nature precludes birefringent phasematching. GaAs and other potentially useful zincblende semiconductors like ZnSe are not ferroelectric and no techniques analogous to electric field poling in $LiNbO_3$ exist for inducing a quasi-phase-matching (QPM)[1] domain grating in an already grown crystal. This QPM problem was solved first by the stack of plates approach[2] and made practical with the addition of wafer bonding.[3,4] This approach proved successful and capable of generating crystals of large aperture, but remains limited, as it is a serial fabrication process. In addition, fabricating very short period gratings by these techniques is extremely challenging. First order QPM of parametric processes pumped at $\lambda = 1.064$, 1.55, and 2.1 μm require domain periods around $\Lambda = 9$, 27, and 60 μm, respectively, where the period Λ and coherence length l_c are defined as

$$\Lambda = 2l_c = \left(\frac{n_p}{\lambda_p} - \frac{n_s}{\lambda_s} - \frac{n_i}{\lambda_i}\right)^{-1} \quad (1)$$

using the wavelengths λ and refractive indices n of the pump, signal, and idler waves.

Techniques have also been developed which make possible the epitaxial growth of orientation-patterned semiconductor films using either wafer-bonded templates[5] or all-epitaxially fabricated templates.[6,7] Work to date has focused on waveguide devices, but the same techniques can produce orientation templates for growth of films thick enough for focusing gaussian beams through the film aperture. Bulk focusing through thick apertures eliminates the limitations on power handling that result from the small apertures of waveguide devices. Beaucarn *et al.*[8] have demonstrated growth of GaAs orientation-patterned layers on polished wafer-bonded stacks of plates. Combining epitaxial template technology and thick GaAs growth enables a more practical approach to fabrication of thick orientation-patterned GaAs films. We report here the fabrication of 200-μm-thick orientation-patterned GaAs (OPGaAs) films and demonstrate the feasibility of growing apertures suitable for bulk frequency conversion with excellent domain quality. We have performed frequency doubling of CO_2 laser radiation with near theoretical efficiency in these films and observe good optical transmission in the near and mid-IR.

The OPGaAs films are fabricated by a multistep process illustrated in Fig. 1. First, GaAs/Ge/GaAs heteroepitaxy[6] is used to create an inverted or antiphase GaAs layer on a GaAs substrate [Fig. 1(a)], after which this wafer is patterned to create an orientation template [Fig. 1(b)]. This template then undergoes two epitaxial growth steps to produce the thick OPGaAs film [Figs. 1(c) and 1(d)].

More specifically, a 1-μm-thick GaAs/$Al_{0.8}Ga_{0.2}As$ superlattice buffer terminating in a final 1000 Å GaAs layer is grown by molecular beam epitaxy (MBE) on a (100) GaAs wafer misoriented 4° towards (111)B. The superlattice buffer is required to prevent roughening of the wafer surface during growth. A 30 Å Ge layer is then grown on top of the GaAs at 350 °C, followed by exposure to an As_2 prelayer at 500° and growth of a 200 Å GaAs layer at 500 °C whose crystallographic orientation is rotated 90° around the [100] direction with respect to the substrate, equivalent to an inversion in the $\bar{4}3m$ zincblende structure. Finally, a top 500 Å $Al_{0.8}Ga_{0.2}As$ layer is grown to protect the underlying GaAs from contamination. All MBE growth was performed using a Varian Gen II MBE system with a valved arsenic cracker. Exposure and development of a photoresist etch mask followed by chemi-

[a]Electronic mail: eyres@loki.stanford.edu
[b]Present address: NetTest, 52 Avenue de l'Europe, 78160 Marly Le Roi, France.
[c]Present address: Wafertech, 5509 N. W. Parker St., Camas, Washington 98607.
[d]Present address: Alcate Submarine Networks, Route de Villejst, 91625 Nozay Cedex, France

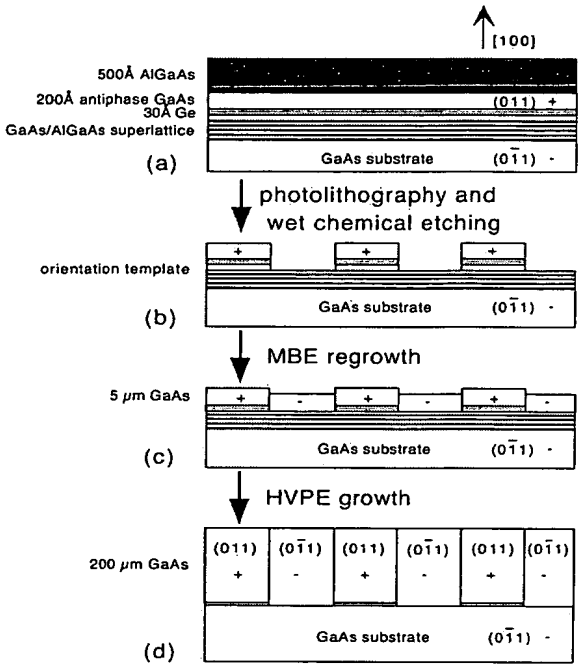

FIG. 1. Fabrication process for thick orientation-patterned GaAs. ± indicates both the polarity of the GaAs layers and the sign of the nonlinear susceptibility.

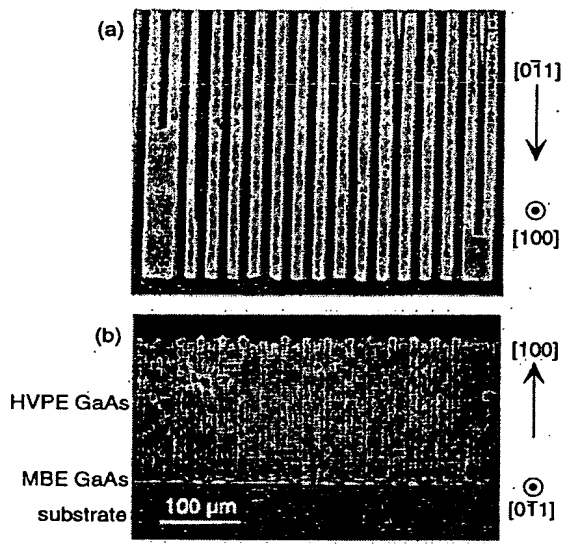

FIG. 2. Top view (a) and stain-etched cross section (b) of 200-μm-thick orientation-patterned GaAs film with 27 μm grating period. Crystal orientations shown are those of the substrate.

cal etching down to the substrate produces an orientation grating pattern across the wafer surface. Employing a selective etch (citric acid/hydrogen peroxide in a 4:1 ratio),[9] we stop at the top $Al_{0.8}Ga_{0.2}As$ etch stop layer of the superlattice, after which the top protective $Al_{0.8}Ga_{0.2}As$ and the etch stop are removed using 1:1 HCl/H_2O. A final brief dip in H_2O_2 followed by 1:1 $HCl:H_2O$ was necessary to eliminate aluminum-containing residues which caused large defect densities in regrown films. XPS analysis of the wafer surface before the additional H_2O_2 dip revealed enhanced Al and O concentrations which disappeared after additional dipping in H_2O_2 and $HCl:H_2O$. The patterned orientation template produced by this process [Fig. 1(b)] was then placed back into the MBE system for growth of 5 μm GaAs as a seed layer for subsequent thick GaAs growth.

Hydride vapor phase epitaxy (HVPE) growth was performed using a conventional $AsH_3/Ga+HCl/H_2$ transport system. The hot-wall horizontal quartz reactor has two inlets, one for flow of $HCl+H_2$ over the 7N Ga source (providing GaCl) and the other for AsH_3, H_2 carrier flow, and additional HCl. Total flow is about 1 slm. The temperatures of the Ga source and of the GaAs substrate were 850 and 750 °C respectively, and the growth occurred at atmospheric pressure. The vertical growth rate was about 10 μm/h. By varying the vapor phase composition (III/V) ratio between 3 and 10), different stable lateral sidewall facets, either {011} or {111}, have been demonstrated in selective-area-masked stripe growth on (100) surfaces by HVPE.[10] For the present experiments we used the growth conditions suitable for {011} sidewalls, which resulted in vertical antiphase domain boundaries.

Figures 2(a) and 2(b) show a top view and stain-etched cross-section of a 200-μm-thick OPGaAs film with an antiphase domain period of 27 μm (13.5 μm wide domains). The **k** vector of the orientation grating is aligned along the substrate [011] so the antiphase boundaries (APBs) lie nominally in {011}. The APBs propagate almost exclusively vertically, which preserves the intended domain duty cycle during HPVE growth. With the stable domain propagation observed here, it is reasonable to consider growth of millimeter scale films with similar domain periods. OPGaAs films with gratings aligned in the orthogonal direction (grating **k** vector along the substrate [0$\bar{1}$1]; down the surface atomic steps) are significantly rougher and have lower domain quality. Probably the presence of APBs impedes the propagation of atomic steps across the surface during epitaxial growth and leads to larger corrugations and enhanced probability of domain overgrowth.

Two domains visible in Fig. 2 are interrupted, with the cross section indicating that the domains close over suddenly after growing vertically for much of the film thickness. Examination of the film surface and polished domain cross sections indicates that most of these interruptions originate at the template and increase linearly in length with increasing film thickness. Template defects which could nucleate the interruptions include lithographic defects, oval defects in the MBE-grown films, or contamination resulting from the wet processing.

End facets were polished on [011] faces of a 4.6 mm long piece of OPGaAs having the 212 μm domain period required for frequency doubling of 10.6 μm radiation. The CO_2 laser beam was focused to a 50 μm waist using BaF_2 lenses to make it approximately confocal in the OPGaAs crystal. Using the GaAs refractive index model of Ref. 11, we can calculate the expected sample transmission including two Fresnel reflections to be 51.4%. The maximum measured transmission at 10.5 μm was 50.6%. More accurate attenuation measurements await thicker OPGaAs apertures where

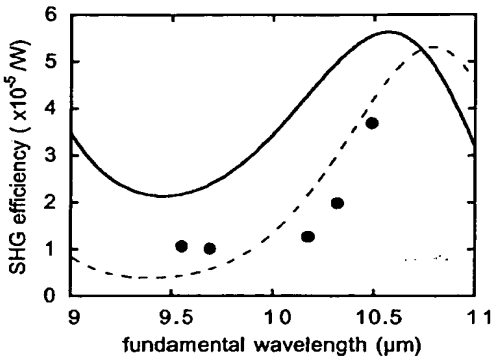

FIG. 3. Internal second harmonic generation efficiency as a function of fundamental wavelength for 4.6 mm long OPGaAs film with 212 μm domain period. Continuous line shows efficiency predicted using refractive index model in Ref. 11; dashed line is theoretical efficiency with additional dispersion shift of $\Delta n = 0.0003$.

beam clipping at the top air/GaAs interface and highly doped substrate can be eliminated. For second harmonic generation a sapphire plate was used to filter out the fundamental radiation before the second harmonic signal passed through a chopper and onto a pyroelectric detector. The pump radiation was polarized in the plane of the film ([110]), while the generated second harmonic was polarized orthogonal to that direction ([001]) as determined by the symmetry of d_{14}.

Figure 3 shows the measured internal harmonic generation efficiency as a function of fundamental wavelength. The solid line is the tuning predicted with the dispersion relation of Ref. 11. The prediction is quite sensitive to small changes in the dispersion; increasing the dispersion between fundamental and harmonic by $\Delta n = 0.0003$ results in the dashed curve. Note that Ref. 11 reports a rms refractive index deviation between data and model of ~ 0.004, larger than that necessary to explain the discrepancy between model and data. Extending the measurement to 11 μm would have helped resolve the ambiguity in the dispersion behavior, but the CO_2 laser available for the experiment could not be tuned beyond 10.5 μm. A lower bound on the effective nonlinear coefficient can be obtained by assuming the 10.6 μm data point represents the peak of the tuning curve. The result is 47 pm/V. If the dispersion relation used to generate the dashed curve is correct, the best fit value is 55 pm/V. The predicted value assuming $d_{14} = 90$ pm/V is $d_{\text{eff}} = (2/\pi) * d_{14} = 57$ pm//V.

We have demonstrated the growth of thick orientation-patterned GaAs films using all-epitaxial techniques and the frequency doubling of a CO_2 laser in those films. The antiphase boundaries between regions of opposite orientation propagate vertically under HVPE growth conditions so that the domain duty cycle is preserved. The observed vertical domain propagation with short domain periods offers strong reasons for optimism about fabricating millimeter-scale films with the thin domains required for quasi-phase-matched frequency conversion of mid-IR radiation.

The authors thank Dmitrii Simanovskii and Daniel Palanker for use of their CO_2 laser and Chris Remen for polishing GaAs samples. This material is based upon work supported by the U.S. Army Research Office under ARO Contract No. DAAH04-96-1-0002. Research was also supported by AFOSR under Grant F49620-99-1-270.

[1] M. M. Fejer, G. A. Magel, D. H. Jundt, and R. L. Byer, IEEE J. Quantum Electron. **28**, 2631 (1992).
[2] A. Szilagyi, A. Hordvik, and H. Schlossberg, J. Appl. Phys. **47**, 2025 (1976).
[3] D. Zheng, L. A. Gordon, Y. S. Wu, R. S. Feigelson, M. M. Fejer, and R. L. Byer, Opt. Lett. **23**, 1010 (1998).
[4] E. Lallier, L. Becouarn, M. Brevignon, and J. Lehoux, Electron. Lett. **34**, 1609 (1998).
[5] S. J. B. Yoo, C. Caneau, R. Bhat, M. A. Koza, A. Rajhel, and N. Antoniades, Appl. Phys. Lett. **68**, 2609 (1996).
[6] C. B. Ebert, L. A. Eyres, M. M. Fejer, and J. S. Harris, J. Cryst. Growth **201/202**, 187 (1999).
[7] S. Koh, T. Kondo, M. Ebihara, T. Ishiwada, H. Sawada, H. Ichinose, I. Shoji, and R. Ito, Jpn. J. Appl. Phys., Part 2 **38**, L508 (1999).
[8] L. Becouarn, B. Gerard, M. Brevignon, J. Lehoux, Y. Gourdel, and E. Lallier, Electron. Lett. **34**, 2409 (1998).
[9] M. Tong, D. G. Ballegeer, A. Ketterson, E. J. Roan, K. Y. Cheng, and I. Adesida, J. Electron. Mater. **21**, 9 (1992).
[10] E. Gil-Lafon, J. Napierala, D. Castelluci, A. Pimpinelli, R. Cadoret, and B. Gerard, J. Cryst. Growth **222**, 482 (2001).
[11] A. N. Pikhtin and A. D. Yas'kov, Sov. Phys. Semicond. **12**, 622 (1978).